Fundamental Limits of Nonreciprocal Plasmonic Metasurfaces

Xu Han[1] and J Sebastian Gomez-Diaz[1]

[1]Affiliation not available

December 18, 2023

Abstract

This work unveils the fundamental limits of linear and nonreciprocal plasmonic metasurfaces in terms of isolation and loss. The proposed bounds are related to surface waves and only depend on the nonreciprocal material employed within the metasurface, thus being independent of geometrical considerations and the presence of other materials. We apply these fundamental limits to explore two different platforms, namely drift-biased and magnetically-biased graphene metasurfaces. For each platform, we first analytically derive the upper bounds in terms of graphene conductivity. Then, we explore devices proposed in the literature and benchmark their response against their upper bounds. Results highlight that drift-biased hyperbolic metasurfaces exhibit outstanding performance in the mid-infrared region, whereas magnetically-biased devices are better suited for the low terahertz band. More broadly, our bounds allow to quickly assess the performance of nonreciprocal plasmonic metasurfaces with respect to their fundamental limit, thus streamlining the device design process and preventing that significant efforts are dedicated to marginal performance improvements. The proposed bounds pave the way toward the development of quasi-optimal nonreciprocal metasurfaces, with important applications in sensing, imaging, communications, and nonlinear optics, among many others.

Fundamental Limits of Nonreciprocal Plasmonic Metasurfaces

Xu Han and J. Sebastian Gomez-Diaz, *Senior Member, IEEE*

***Abstract*—This work unveils the fundamental limits of linear and nonreciprocal plasmonic metasurfaces in terms of isolation and loss. The proposed bounds are related to surface waves and only depend on the nonreciprocal material employed within the metasurface, thus being independent of geometrical considerations and the presence of other materials. We apply these fundamental limits to explore two different platforms, namely drift-biased and magnetically-biased graphene metasurfaces. For each platform, we first analytically derive the upper bounds in terms of graphene conductivity. Then, we explore devices proposed in the literature and benchmark their response against their upper bounds. Results highlight that drift-biased hyperbolic metasurfaces exhibit outstanding performance in the mid-infrared region, whereas magnetically-biased devices are better suited for the low terahertz band. More broadly, our bounds allow to quickly assess the performance of nonreciprocal plasmonic metasurfaces with respect to their fundamental limit, thus streamlining the device design process and preventing that significant efforts are dedicated to marginal performance improvements. The proposed bounds pave the way toward the development of quasi-optimal nonreciprocal metasurfaces, with important applications in sensing, imaging, communications, and nonlinear optics, among many others.**

***Index Terms*—Fundamental limits, graphene, metasurfaces, nonreciprocity, plasmonics.**

I. INTRODUCTION

BREAKING reciprocity lies in the heart of modern electromagnetic devices such as circulators [1]-[4], isolators [5]-[7], filters [8], [9], and antennas [10]-[12]. Generally, breaking reciprocity can be realized by biasing the device with a physical quantity that is odd-symmetric under time-reversal [13]. Conventionally, such response has been achieved by magnetically biasing ferromagnetic compounds and garnets [14], [15]. In the past decade, magnetless approaches based on nonlinear responses, spatiotemporal modulation, drifting electrons, and opto-mechanical effects have been explored across the electromagnetic spectrum [16]-[27]. In a related context, the field of plasmonics has opened new possibilities to control and manipulate light beyond the diffraction limit [28] and has enabled countless applications in areas such as sensing, spectroscopy, and healthcare [29]-[31]. Surface plasmon polaritons (SPPs) are electromagnetic modes confined to two-dimensional (2D) interfaces that possess evanescent fields in the direction perpendicular to the interface. For instance, SPPs are supported by dielectric-metal interfaces at infrared (IR) and visible frequencies [32] and by graphene and other 2D materials [33]-[36] in the terahertz (THz) and IR bands. The emerge of ultrathin metasurfaces [37] and 2D materials [38] have provided new knobs to excite, process, and route SPPs, while also enabling unexpected possibilities to manipulate and enhance nonreciprocal responses [39]-[41] Nonreciprocal plasmonics lead to strong light-matter interactions[42], useful in areas as nonlinear wave generation, sensing, and communications, among others. Unfortunately, the design of quasi-optimal nonreciprocal metasurfaces is usually quite challenging and require significant computational resources. Given the abundant choice of materials and large degree of freedoms for geometrical shapes and dimensions, it would be highly desirable to determine the optimal response that can be achieved by a metasurface loaded with a specific nonreciprocal material. This would allow to (i) streamline the design process, by assessing the performance of a given device with respect to the fundamental bounds; and (ii) prevent that significant efforts are dedicated to marginally improve the device performance while leading to unnecessarily complex structures.

The fundamental limits and trade-offs between isolation and loss of a waveguide junction filled with an arbitrary dielectric was derived in the 50s [43]. More specifically, when a two-port network containing a nonreciprocal magnetic material is magnetized by an external field, there are upper bounds only associated with the magnetic material. Such bounds determine a figure of merit (FoM) for the entire device performance, are independent of geometrical considerations and the presence of other materials, and lead to a clear trade-off between isolation and loss. This elegant result is readily applicable to modulators and can easily be extended to nonreciprocal devices working with propagative waves. Based on this work, the fundamental limits of a realistic optical switching device showed that its dynamic performance is only subjected to the tunable material employed within the device [44]. In 2014, this approach was applied to determine the fundamental limits of magnetically-biased graphene-based devices interacting with waves propagating in free-space [45]. Several configurations, including isolators and Kerr rotators, were investigated for random planar device geometries within a large parametric space. It was shown that some specific devices, with tailored nanostructures made of graphene and metals, can reach performances very close to the upper fundamental limits offered by magnetically-biased graphene. To date, fundamental

This work was supported in part by the Keck Foundation and by the National Science Foundation with a CAREER Grant No. ECCS-1749177.

X. Han and J. Sebastián Gómez-Díaz are with the Department of Electrical and Computer Engineering, University of California, Davis. Davis, California 95616 USA. (e-mail {xhhan, jsgomez}@ucdavis.edu).

Color versions of one or more of the figures in this article are available online at http://ieeexplore.ieee.org

bounds of nonreciprocal devices are limited to *propagative* waves and cannot be applied within the field of plasmonics.

In this paper, we study and unveil the fundamental bounds of linear, nonreciprocal plasmonic metasurfaces, as those illustrated in Fig. 1. These bounds only depend on the nonreciprocal material that fill the devices and can be obtained analytically for some configurations. Our approach is general in the sense that account for different mechanisms to obtain nonreciprocity, including magnetic bias and nonlocality (for instance, obtained using drifting electrons). To this purpose, we first review the isolation equation as initially proposed in Ref. [43] and define a metric to evaluate the performance of nonreciprocal plasmonic metasurfaces in terms of isolation and loss. Then, we apply an effective medium approach (EMA) [46] to relate ultrathin metasurfaces and bulk media, which in turn permit us to obtain the upper bound of the structures in the non-retarded regime. Next, we study two different nonreciprocal plasmonic platforms: drift-biased and magnetically-biased graphene metasurfaces. For each scenario, we derive analytical upper bounds that only depend on graphene's conductivity and then we explore realistic metasurfaces studied in the literature and benchmark their performance against the bounds. Our study reveals that drift-biased hyperbolic metasurfaces have a tremendous potential for nonreciprocal plasmonics in the mid-IR, while magnetically-biased metasurfaces are better suited for the low terahertz (THz) band. More broadly, our approach can readily be applied to assess the performance of plasmonic metasurfaces composed of any nonreciprocal material, including magneto-optical [47] and 2D materials [42], and paves the way to quick development of optimal nonreciprocal devices.

II. ISOLATION INEQUALITY

Let us consider a linear two-port network filled with arbitrary materials. Let us also consider that, upon applying any odd physical quantity (biasing), one of the materials inside of network becomes nonreciprocal. To evaluate the performance of the network, we employ the following FoM [43]

$$\gamma_{isol}(\underline{S}_A, \underline{S}_B, \boldsymbol{a}_A, \boldsymbol{a}_B) \triangleq \frac{\left|\boldsymbol{a}_B{}^T(\underline{S}_A - \underline{S}_B{}^T)\boldsymbol{a}_A\right|^2}{\boldsymbol{a}_A{}^H(\underline{I} - \underline{S}_A{}^H\underline{S}_A)\boldsymbol{a}_A \cdot \boldsymbol{a}_B{}^H(\underline{I} - \underline{S}_B{}^H\underline{S}_B)\boldsymbol{a}_B}, \quad (1)$$

where $\underline{S}_{A,B}$ is the scattering matrix of the network, $\boldsymbol{a}_{A,B}$ is a vector containing the excitation waves, $\underline{I}$ is the identity matrix, and the superscript T and H denote transpose and Hermitian transpose operators, respectively. Additionally, the subscripts A and B represent two distinct states of the device that are being considered to evaluate nonreciprocity. Intuitively, Eq. (1) provides an idea of the device nonreciprocal response (numerator) versus the power dissipated in these scenarios (denominator), i.e., a trade-off between the isolation and loss. Remarkably, the values of the FoM are delimited by an upper bound dictated only by the intrinsic properties of the nonreciprocal material filling the device. This leads to the following isolation inequality [45]:

$$\gamma_{isol}(\underline{S}_A, \underline{S}_B, \boldsymbol{a}_A, \boldsymbol{a}_B) \leq \gamma_{max}. \quad (2)$$

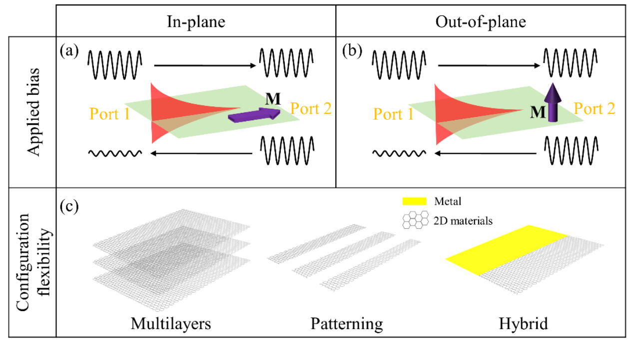

Fig. 1. Nonreciprocal plasmonic metasurfaces based on 2D materials. The metasurfaces can be biased with an external momentum applied parallel (a) or perpendicular (b) to the structures. (c) Some potential degrees of freedom to construct plasmonic metasurfaces, including the use of multilayers of 2D materials, nanopatterning, and the inclusion of other materials such as metals or dielectrics.

In the common case that the electric properties of the material (i.e., its permittivity tensor $\underline{\varepsilon}$) enable the nonreciprocal response, the upper bound γ_{max} is the largest eigenvalue of $\left(\underline{\varepsilon}_A^T - \underline{\varepsilon}_A^*\right)^{-1}\left(\underline{\varepsilon}_B^* - \underline{\varepsilon}_B^*\right)^{-1}\left(\underline{\varepsilon}_A - \underline{\varepsilon}_B^T\right)\left(\underline{\varepsilon}_B^* - \underline{\varepsilon}_A^H\right)$ [43]. When the network is used to maximize isolation, the incident waves associated to states A and B can be defined as $\boldsymbol{a}_A = (1 \quad 0)^T$ and $\boldsymbol{a}_B = (0 \quad 1)^T$, i.e., the device is only excited from the left or right port of the two-port network. This allows to simplify the FoM to

$$\gamma_{isol}(|S_{12}|, |S_{21}|) = \frac{(|S_{21}| - |S_{12}|)^2}{(1 - |S_{21}|^2)(1 - |S_{12}|^2)}, \quad (3)$$

where S_{21} and S_{12} are the transmission coefficients from port 1 to 2 and from port 2 to 1, respectively. To better illustrate the tradeoff between isolation and loss, the FoM can be expressed as

$$\gamma_{isol}(I, L) = \frac{L^2(1 - I)^2}{(1 - L^2)(I^2 - L^2)} \quad (4)$$

where $I = |S_{21}|/|S_{12}|$ is the isolation between the network ports, and $L = |S_{21}|$ is associated to the insertion loss assuming $|S_{21}| > |S_{12}|$ and perfect matching. To gain physical insight into this concept, let us consider a set of 2 port networks, all of them loaded with an identical nonreciprocal material and subjected to the same momentum bias. The performance of all networks, no matter how complex they are and what other materials they employ, will be upper bounded by γ_{max}. This bound only depends on the nonreciprocal material employed in the networks and determines the minimum loss that can be attainable in practice to achieve an isolation level I. Then, each specific network will benchmark a different performance γ_{isol} that shows how close its behavior is with respect to the fundamental limit, with $\gamma_{isol} \leq \gamma_{max}$.

In order to apply these bounds to the field of plasmonics, we consider a nonlocal and frequency-dispersive and ultrathin metasurface characterized by a fully populated conductivity tensor [48]-[50]

$$\underline{\sigma}(\omega,\boldsymbol{k}) = \begin{bmatrix} \sigma_{xx}(\omega,\boldsymbol{k}) & \sigma_{xy}(\omega,\boldsymbol{k}) \\ \sigma_{yx}(\omega,\boldsymbol{k}) & \sigma_{yy}(\omega,\boldsymbol{k}) \end{bmatrix}, \tag{5}$$

where ω is the angular frequency and $\boldsymbol{k}$ is the wavevector of the supported wave. Nonlocality is associated to the different response that the nonreciprocal material can potentially exhibit as a function of the momentum of the supported waves [48],[51] and, as detailed in further detail below, it is key to describe nonreciprocal systems based on drifting electrons [52],[53]. Using an effective medium approach [54], the metasurface can also be characterized as a thin dielectric layer of thickness d with a nonlocal effective permittivity tensor $\underline{\varepsilon}$,

$$\begin{gathered} \varepsilon_{zz} = \varepsilon_0, \\ \varepsilon_{xx(\,yy)}(\omega,\boldsymbol{k}) = 1 - j\sigma_{xx(yy)}(\omega,\boldsymbol{k})/(\omega d), \\ \varepsilon_{xy(yx)}(\omega,\boldsymbol{k}) = -j\sigma_{xy(yx)}(\omega,\boldsymbol{k})/(\omega d). \end{gathered} \tag{6}$$

In the non-retarded regime (i.e., $|\boldsymbol{k}| \gg |\boldsymbol{k}_0|$, where $\boldsymbol{k}$ and $\boldsymbol{k}_0$ are the wavevectors of the supported SPPs and free space, respectively), the SPPs fields are strongly confined to the metasurface and exhibit rapidly decaying evanescent fields. In that scenario, the upper bounds of plasmonic metasurfaces can effectively be determined by analyzing the fields inside the effective anisotropic slab and determining their upper bound γ_{max} . In the following, we apply this approach to comprehensively explore two different nonreciprocal plasmonic platform, namely drift- and magnetically- biased graphene, and to analytically derive their fundamental limits as a function of graphene's properties and the applied momentum.

III. Application to Drift-Biased graphene plasmonics

An effective way to achieve broadband nonreciprocal SPPs propagation is by applying drift current to graphene-based metasurfaces [55]-[58]. Since SPPs are collective oscillations of charges interacting with light, their propagation features are strongly affected by DC current. Drifting electrons with a velocity v_d either drag or oppose the SPPs, inducing a Doppler-shifted wavenumber [53],[59]. As a result, SPPs effectively see different media when propagating along and against the drift current, leading to broadband nonreciprocity [26]. Recently, drift-biased graphene plasmonics have been experimentally demonstrated [51],[60] and attracted significant attention for various applications, including nonlinear wave generation [42] and hyperlensing [58].

A drift-biased graphene platform is schematically shown in the inset of Fig. 2(a). Graphene is transferred onto a dielectric substrate (SiC [61],[62]) and two metallic electrodes (yellow bars) are printed to create electrical contact. By applying an external DC voltage across the metals, graphene is longitudinally biased by drifting electrons travelling from one electrode to the other with a velocity $\vec{v}_d = v_d\hat{y}$. Such velocity depends on the distance between the electrodes as well as graphene properties in terms of chemical potential (μ_c) and relaxation time (τ), and it is always below the Fermi velocity of electrons in graphene ($v_F \approx 10^6$ m/s). In this scenario, graphene becomes nonlocal because its response depends on the momentum of the supported waves. Such response can be

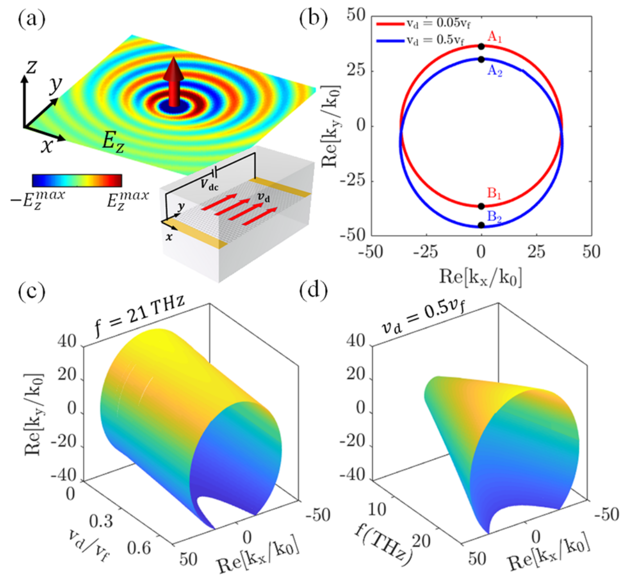

Fig. 2. Drift-biased graphene as a nonreciprocal plasmonic metasurface. (a) Schematic showing the z-component of electric field excited by a z-oriented dipole (red arrow) located at 100 nm over a drift-biased ($v_d = 0.5\, v_F$) graphene at 21 THz. Inset shows the device schematic. (b) Isofrequency contour of the states supported by graphene at 21 THz for two different velocities of drifting electrons. (c) and (d) Momentum of the supported states versus drift velocity and frequency, respectively. Other parameters are $\tau = 0.1\,ps$ and $\mu_c = 0.4\,eV$.

modelled using a conductivity tensor $\underline{\sigma} = (\sigma_g \quad 0;\ 0 \quad \sigma_d)$ [53], where σ_g is graphene's conductivity without the drift bias [63] and $\sigma_d(v_d,k_y) = [\omega/(\omega - k_y v_d)]\sigma_g(\omega - k_y v_d)$, with k_y being the wavevector component along the drift [55]. Nonreciprocity follows because reversing the wave travelling direction effectively means flipping the electron drifting direction, resuling in $\sigma_d(v_d,+k_y) \neq \sigma_d(v_d,-k_y)$. Probably the simpler approach to excite SPPs in this platform is to locate a z-oriented dipole in its near-field. We analyze this scenario using a home-made anisotropic Green's function approach developed in Ref. [53]. The z-component of the SPP's electric field excited by a dipole located at 100 nm over the metasurface is shown in Fig 2(a). Results show that the dipole excites waves propagating along all directions within the plane. For directions transverse to drifting electrons, i.e., $\pm x$, SPPs show a symmetric field profile. Nonreciprocity appears along the y axis, i.e., along the direction of the applied DC bias. Plasmons traveling along $+y$ are less confined that along other directions and travel longer with little loss. Remarkably, SPPs directed against the current (i.e., $-y$) are very confined and lossy, thus quickly decaying. Fig. 2(b) shows the isofrequency contour (IFC) of the waves supported by the platform for two different velocities of the drifting electrons. Results confirm that, as the drift velocity increases, the IFC asymmetry along k_y increases, thus leading to larger nonreciprocal responses. Points A and B in the IFC plots are associated to the wavenumber of the SPPS traveling along and against the current, respectively. Fig. 2(c)-(d) completes our analysis by providing a parametric study of the momentum of the supported SPPs versus drift velocity and frequency, confirming that nonreciprocity may appear over a large bandwidth.

To find the fundamental limits of drift-biased graphene-based metasurfaces, we analytically derive the isolation inequality as

$$\frac{L^2(1-I)^2}{(1-L^2)(I^2-L^2)} \leq \frac{\left|\sigma_{yy}(v_d,k_{Ay})-\sigma_{yy}(v_d,k_{By})\right|^2}{\sigma'_{yy}(v_d,k_{Ay})\sigma'_{yy}(v_d,k_{By})} = \gamma_{max}, \quad (7)$$

where the superscript $'$ denotes the real parts of the conductivity component. In Eq. (7), the left-hand side is related to the performance of a given plasmonic device in terms of loss and isolation. The right-hand side provides the upper performance (γ_{max}) that can be attained by any metasurface that host drift-biased graphene with certain features (i.e., chemical potential, relaxation time, temperature, and velocity of drifting electrons). Remarkably, only the conductivity term associated to the drift (σ_{yy}) appears in the bound. This is because the system is reciprocal along the x-direction, and thus σ_{xx} does not directly contribute to the system nonreciprocity. Maximum isolation will be obtained between states A and B, i.e., between waves travelling along and against the drifting electrons. We denote the wavenumber of such waves as k_{Ay} and k_{Ay}, respectively. Even though nonreciprocity will also appear for waves propagating toward other directions, their nonreciprocal behavior will be weaker and thus such performance will fall within our bound. In a general scenario, the effective nonlocal σ_{yy} conductivity of the metasurface will strongly depend on the properties of the supported waves, which in turn can be manipulated using metal, patterning, and different geometries [39],[40]. An optical metasurface structure could be designed to exploit the platform at their limits, i.e., when $k_{Ay} \rightarrow k_0$ and when $k_{By} \rightarrow \infty$. In practice, graphene does not support waves with a confinement beyond $300k_0$ due to intrinsic nonlocal effects [64]-[66], thus a conservative value of $k_{By} \approx 100\, k_0$ is considered here. As a result, $k_{Ay} = k_0$ and $k_{By} = 100\, k_0$ impose the boundaries for the isolation inequality in Eq. (7) for an optimal structure.

Fig. 3 illustrates the fundamental bounds and optimal device performance obtained by drift-biased graphene-based plasmonic metasurfaces at 21 THz. Panel (a) overviews the isolation-loss plot employed to benchmark the device performance: blue area denotes the forbidden region, associated to a performance that surpass our bound, and white area denotes a performance that can be obtained by realistic metasurfaces. The dark blue circle marks the best performance that can be obtained with a material. This study is extended in Fig. 3(b) for different velocities of the drifting electrons. Results suggest that significant isolation levels, over 25 dB, can be obtained with minimal loss (<1 dB) and moderate drift-bias. The fundamental limits (isolation/loss) of this type of metasurfaces are parametrically explored in Fig. 3(c)-(d) for two different drift velocities versus frequency. Results confirm that this type of devices have the potential to exhibit an excellent performance over a broad frequency range. It should be stressed this platform exhibit better performance as frequency increases, and thus it is better suited to operate in the mid-IR band than at low THz frequencies. Additionally, it can be observed that isolation/loss trade-offs significantly improve as the velocity of the drifting electrons increases. The challenge now is to design quasi-optimal plasmonic metasurfaces able to benchmark close to

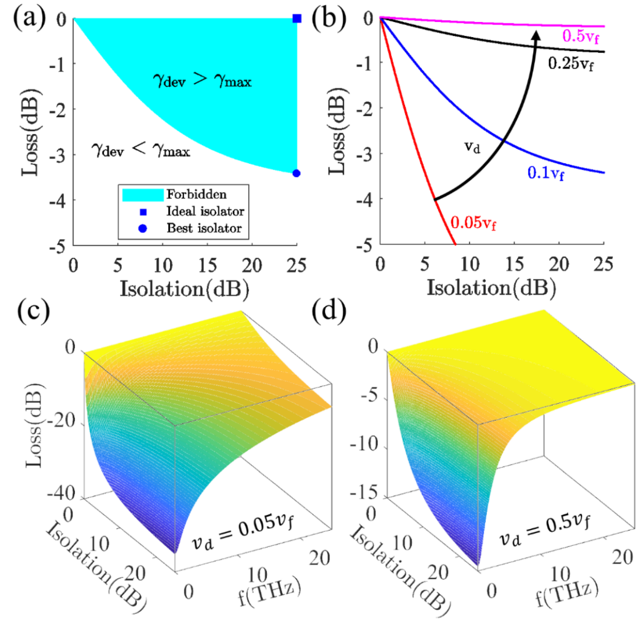

Fig. 3. Fundamental bounds of drift-biased graphene metasurfaces. (a) Concept of isolation inequality. Any plasmonic device using drift-biased ($v_d = 0.1v_f$) graphene at 21 THz will exhibit a response in terms of loss and isolation within the white area of the panel. Blue area represents device performance that cannot be reached. (b) Isolation inequality for various drift velocities of flowing electrons for a graphene-based metasurface at 21 THz. Panels (c) and (d) show the isolation inequality versus frequency for drift velocities $v_d = 0.05v_f$ and $v_d = 0.5v_f$, respectively. Other parameters are as in Fig. 2.

these bounds. In the following, we explore and benchmark the performance of two different platforms: a graphene-sheet employed as a 1D transmission line, a configuration described elsewhere [35],[67] to construct plasmonic devices such as switches or filters, and isotropic and hyperbolic drift-biased metasurfaces [51],[60], [73] excited by a dipole source.

To gain a better understanding of the bounds of drift-biased graphene, we develop a transmission line (TL) [35],[67] composed of three sections of graphene in which only the center one is drift-biased (see Fig. 4). This allows to further isolate the response of drift-biased graphene with respect to the excitation. We model this structure in COMSOL Multiphysics [68]. To this purpose, we calculate the drift-biased conductivity of graphene with wavenumbers along and against the drift electrons, and we used them to construct two simulation models: one associated to forward SPP propagation (along the drift) and other for backward SPP propagation (against the drift). We treat the side regions of the structure as ports, and characterize them using lossless, unbiased, graphene. The z-components of the electric field for SPPs travelling in such TL system are depicted in Fig. 4(a). For forward propagation ($+y$ direction, top panel), SPPs travels through the drift-biased section of graphene without significant changes. However, waves propagating against drifting electrons ($-y$ direction, bottom panel) undergo a change in their wavelength together with very significant damping. We quantified this result by calculating the S_{21} and S_{12} coefficients of the system using TL theory [69], which are in good agreement with those found using COMSOL simulations. Fig. 4(b)-(d) report a performance study varying the length of the center graphene section of the structure ℓ from

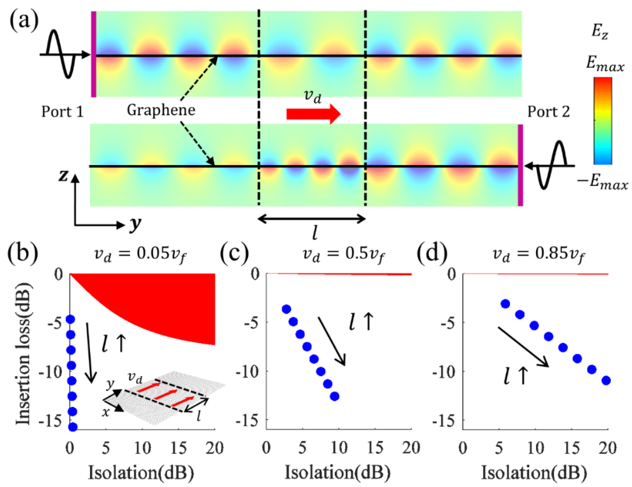

Fig. 4. Drift-biased graphene as a 1D plasmonic isolator. (a) Numerical simulations in COMSOL Multiphysics. The structure is composed of two plasmonic lossless ports made of pristine graphene and one central graphene region of length $\ell = 0.3\mu m$ that has been drift-biased along the direction indicated by the red arrow ($v_d = 0.5v_f$). Results show SPPs propagation along forward (top) and backward (bottom) directions. (b)-(d) Device performance (loss/isolation) for various drift-velocities at 21 THz (blue dots). The length of the drifted section increases from 0.3 μm to 1 μm in steps of 0.1 μm. Cyan regions show the performance bound provided by the isolation inequality. Other parameters are as in Fig. 2.

0.3 to 1 μm. As expected, larger sections provide larger isolation and loss. Increasing the drift-bias further increases the isolation while reducing the loss on the system, leading a trade-off between length and bias to achieve desired responses. However, the performance exhibited by this platform is in all cases well below the upper limits offered by drift-biased graphene. Therefore, we conclude that this platform is far from ideal to achieve quasi optimal nonreciprocal responses.

A realistic approach to excite drift-biased graphene-based plasmonic metasurfaces is to use a dipole located in the near field of the structure. This can be implemented in practice using scanning-type scanning near-field optical microscopy (s-SNOM) by shining laser on a probe tip located above the metasurface [70]-[72]. The tip gets polarized and behaves as a dipole, scattering evanescent fields that couple to the metasurface in the form of SPPs. Here, we explore this excitation approach using a home-made Green's function approach [53] and evaluate its performance and fundamental limits for two specific drift-biased platforms, namely a graphene sheet and a hyperbolic metasurfaces made of graphene ribbons [73].

Fig. 5(a) shows the Poynting vector of SPPs excited by a z-directed dipole located 35 nm over a drift-biased graphene sheet for two different drift-velocities ($v_d = 0.5v_F$ and $v_d = 0.85v_F$). Here, drifting electrons are traveling in the $+y$ direction. We focus on nonreciprocity between the dipole located at $\vec{r}_0'$ and an observer point located at $\vec{r}_0$. In this context, isolation is defined as the ratio of the squared modulus of electric fields at source/observation pairs (i.e., $|E(\vec{r}_0, \vec{r}_0')/E(\vec{r}_0', \vec{r}_0)|^2$ [53]) and loss as $\mathrm{Im}(\mathrm{k_y})$. Fig. 5(c)-(d) evaluate the performance of this platform along the y-axis (i.e., where maximum isolation occurs) when the distance between source and observation increases from 0.3 to 1 μm with steps of

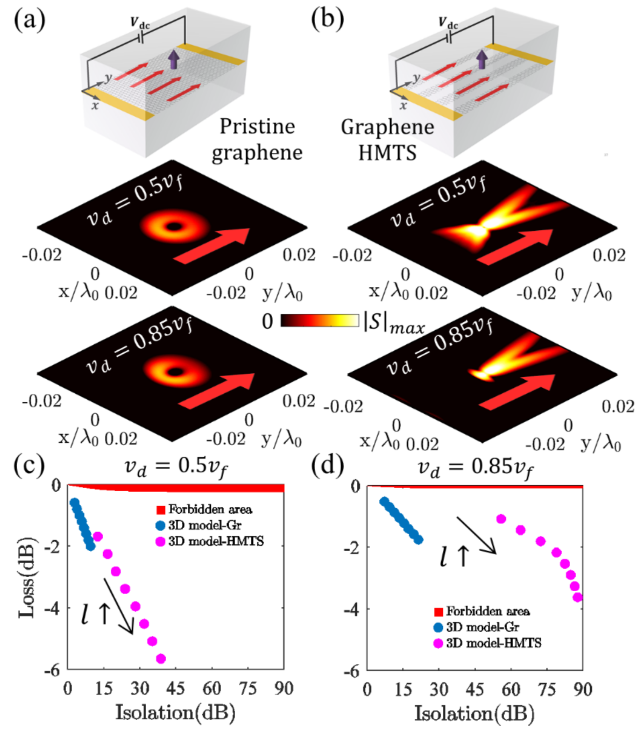

Fig. 5. Electromagnetic response of drift-biased graphene-metasurfaces excited by a z-directed dipole located $z_0 = 35$ nm. Poynting vector (magnitude) of SPPs excited over a drift-biased graphene sheet (a) and a drift-biased hyperbolic metasurface based on an array of graphene ribbons (b). The width and periodicity of the ribbons is set to W=25 nm and L=50 nm, respectively. Results are plotted for two different drift-velocities: $v_d = 0.5v_f$ (central row) and $v_d = 0.85v_f$ (bottom row). Red arrows show the direction of the flowing electrons. (c) Performance in terms of loss and isolation of the metasurfaces shown above for two different drift-velocities, $v_d = 0.5v_f$ (left) and $v_d = 0.85v_f$(right). The length of the drifted metasurfaces increases from 0.3 μm to 1 μm in steps of 0.1 μm. Cyan regions show the performance bound provided by the isolation inequality. Other parameters are as in Fig. 2.

0.1 μm. Results show a trend similar to the one the found in Fig. 4: increasing the drift bias leads to large isolation and lower loss within a somewhat limited range. It should be noted that losses are reduced in this scenario. We attribute such response to the lack of port sections compared to the TL case, and to the overall better matching between the fields radiated by the dipole and graphene. Still, despite these improvements, the performance of the platform is far from reaching the fundamental limits offered by drift-biased graphene.

Finally, we considered a drift-biased graphene-based hyperbolic metasurface composed of a periodic array of graphene ribbons [73]. Fig. 5(b) shows the Poynting vector of SPPs excited by a z-directed dipole located 35 nm over this structure (considering ribbons with width 25 nm and periodicity of 50 nm) for the same drift-velocities studied above. Power profiles show the typical response of hyperbolic structures, with maximum power directed toward oblique angles within the plane. Remarkably, isolation is greatly enhanced in this platform [53]. For sufficiently large drift-velocities, SPPs traveling in the semi-plane against the drift are no longer distinguishable, and thus near-unidirectional propagation immune to backscattering is achieved. Fig. 5 (b)-(c) explore the performance of this platform for different separation distances between source and observation, both defined along the in-plane direction in which SPPs carry maximum power. For moderate drift velocities, $v_d = 0.5v_f$, isolation significantly outperforms the one found in drift-based graphene sheets but at the expense of relatively higher loss. Further increasing the drifting velocity leads to a remarkable performance that benchmarks quite close to the upper bounds of drift-biased graphene. Specifically, isolation levels beyond 50 dB are readily achievable with loss of just 1 dB. Such outstanding response places graphene-based hyperbolic structure as quasi-optimal devices for nonreciprocal plasmonics.

IV. Application to Magnetically-Biased Graphene Plasmonics

Even though many works have explored the interaction of magnetically-biased graphene metasurfaces with plane waves, aiming to construct Faraday rotators [74]-[76] and isolators [77], such structures can also be applied for nonreciprocal plasmonics. For instance, edge-modes propagating on graphene ribbons are nonreciprocal when the structure is combined with metals [78]. However, it is still unclear how optimal such devices are. In general, the vast degrees of freedom to design magnetically-biased graphene metasurfaces make it very challenging to determine if the performance of specific devices is close to the fundamental bounds offered by the material. This usually leads to redundant and time-consuming efforts to marginally increase the device performance by increasing its complexity.

Let us consider a thin arbitrary metasurface that is somehow loaded with magnetically-biased graphene characterized by a conductivity tensor $\underline{\sigma} = (\sigma_d \quad \sigma_H; \ -\sigma_H \quad \sigma_d)$, where σ_d and σ_H correspond to graphene's direct and Hall conductivities component. They can be determined using the Kubo formalism [63]. The isolation inequality that determines the fundamental limits of this platform can be analytically derived as

$$\frac{L^2(1-I)^2}{(1-L^2)(I^2-L^2)} \leq \frac{\sigma_H''^2(B_0)\left[\sigma_H'^2(B_0)+\sigma_H''^2(B_0)\right]}{\left[\sigma_d'^2(B_0)-\sigma_H''^2(B_0)\right]^2} = \gamma_{max}, \qquad (8)$$

where the superscripts $'$ and $''$ denote the real and imaginary parts of the conductivity components, respectively, and B_0 is the magnetic field applied in the direction perpendicular to structure. Similarly to the case studied above, the left-hand side of Eq. (8) is related to the performance (isolation/loss) of a specific plasmonic device whereas the right-hand side provides the upper performance (γ_{max}). Nonreciprocity is here governed by the Hall conductivity of graphene, and the bound reduces to zero in case that the metasurfaces are not magnetically biased, i.e., $\sigma_H \to 0$ forces that $\gamma_{max} \to 0$.

Fig. 6(a) shows the upper bounds (isolation/loss) of magnetically-biased graphene-based metasurfaces at 21 THz versus the applied magnetic field. Results show that large isolation may be achieved with bias as little as 1 T but at the expense of significant loss. Upper performances are significantly improved when larger magnetic bias values are applied. Note that the graphene parameters employed in this panel are identical to those employed in Fig. 3 (b), which allows us to directly compare the performance of drift- and magnetically- biased plasmonic metasurfaces. Fig. 6(b) benchmarks the response of nonreciprocal platforms explored

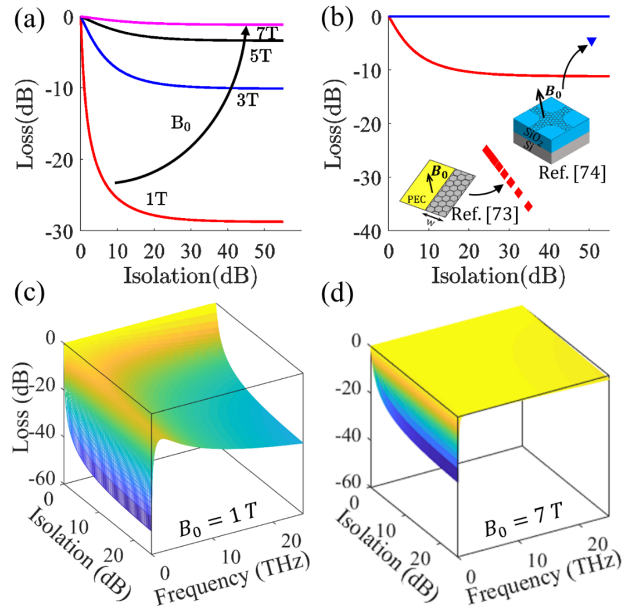

Fig. 6. Upper bounds of magnetically-biased graphene metasurfaces. (a) Upper bounds for various magnetic field values applied on a given graphene sample at 21 THz. (b) Performance analysis of devices studied in the literature, including nonreciprocal edge modes (red diamonds [78]) and a circulator (blue triangle [79]), versus their upper bounds (solid lines). Insets illustrate the devices schematic. (c)-(d) show the isolation inequality versus frequency for applied magnetic fields $B_0 = 1$ T and $B_0 = 7$ T, respectively. Other parameters are as in Fig. 3.

in the literature against the fundamental limits obtained using Eq. (8). Specifically, red data is associated to a nonreciprocal plasmonic system composed of a graphene ribbon that is short-circuited on one edge with a metal plane [78] (see inset). In the system, the ribbon has a width of 100 μm, $B_0 = 1$ T, frequency is set to 2 THz, and graphene's chemical potential and relaxation time are set to 0.37 eV and 0.1 ps, respectively. Nonreciprocal edge plasmons appears on the graphene edge that interfaces with air. The response of the platform is explored changing the length of the graphene ribbon from 0.3 μm to 1 μm with a step of 0.1 μm (red diamonds). Even though the system provides large isolation, it exhibits quite significant loss and benchmarks quite far from the fundamental limits of the material. The other platform considered here is related to the magnetically-biased graphene circulator described in Ref. [79]. It is composed of a cross-shaped graphene pattern (see inset) printed on top of a SiO_2/Si substrate and operates at 3.4 THz. The applied bias is set to $B_0 = 1.5$ T and graphene's chemical potential and relaxation time are set to 0.15 eV and 0.9 ps, respectively. The blue triangle marker displays the performance of the device, which provides significant isolation (~ 50 dB) and moderate loss (~ 5 dB). Even though such performance is remarkable, there is still plenty of room to improve it and bringer close to the upper bounds offered by the magnetically-biased graphene employed in the system.

Fig. 6(c)-(d) further explores the fundamental limits of magnetically-biased graphene as a function of frequency for two magnetic bias, $B_0 = 1$ T and $B_0 = 7$ T. Results show that high performance in terms of isolation/loss can be obtained in the THz band (roughly from ~1 to ~ 5 THz) using moderate bias fields. As frequency increases, the performance significantly degrades, and high isolation is always associated with large loss. Further enhancing the magnetic field to $B_0 = 7$ T allows to construct metasurfaces with excellent trade off in terms of isolation and loss over a large frequency band.

V. Conclusion

In conclusion, we have explored the fundamental limits of nonreciprocal metasurfaces that guide surface waves. Remarkably, these limits are only related to the properties of the nonreciprocal material employed within the device and do not depend on the presence of other materials such as metals or dielectrics or on geometrical considerations. Without loss of generality, we focused on two types of nonreciprocal plasmonic platforms, i.e., drift- and magnetically- biased graphene metasurfaces, and we analytically derived their fundamental bounds. In the case of drift-biased devices, we explored 1D devices excited by surface plasmons using both transmission line theory and full-wave numerical simulations (COMSOL Multiphysics). Additionally, we investigated isotropic and hyperbolic drift-biased metasurfaces excited by electrical dipoles located in the near field of the device – a configuration that mimics s-SNOM microscopy. Our results show that most devices operate relatively far from their upper bounds, and thus their performance can be significantly improved. One important exception is the case of drift-biased hyperbolic metasurfaces, which exhibit an outstanding performance at frequencies close to the mid infrared band. Overall, drift-biased graphene plasmonics is an emerging and promising broadband technology compatible with integrated circuits. In the case of magnetically-biased graphene metasurfaces, we evaluated the performance of several devices studied in the literature – namely an isolator based on nonreciprocal edge modes and a circulator based on patterned graphene – and benchmarked their response against the upper bounds. Even though these devices exhibit very interesting responses, they all operate relatively far from the upper bound and thus their performance can be further improved. Additionally, our bounds revealed that magnetically-biased graphene metasurfaces are well-suited (in terms of isolation/loss trade-offs) to operate in the low terahertz band. Recently, circular dichroism has been demonstrated to be an efficient tool to break reciprocity in 2D materials due to the optically-driven non-degenerate valleys [80]-[82]. As another nonreciprocal plasmonic platform and armed with a similar optical conductivity tensor to that of magnetically-biased graphene, optically-driven 2D materials can also be evaluated though our bounds.

Moving beyond, our bounds can be applied to explore the fundamental limits of many other nonreciprocal plasmonic metasurfaces, including those based on magneto-optic materials [83] and 2D materials such as transition metal dichalcogenide monolayers [84]. We envision that the bounds derived here will be useful in the development of quasi-optimal nonreciprocal metasurfaces employed in areas such as communication, sensing, imaging, and nonlinear optics, among many others.

References

[1] Vani, Divya, et al. "Design And Development of A 6-Port Optical Circulator Using Silicon Photonic Crystals." (2021).
[2] Portela, Gianni, et al. "Photonic integrated circulators based on iron garnets without external magnetization." Smart Photonic and Optoelectronic Integrated Circuits XXIII. Vol. 11690. International Society for Optics and Photonics, 2021.
[3] Wang, Zheng, and Shanhui Fan. "Optical circulators in two-dimensional magneto-optical photonic crystals." Optics letters 30.15 (2005): 1989-1991.
[4] Huang, Duanni, et al. "Dynamically reconfigurable integrated optical circulators." Optica 4.1 (2017): 23-30.
[5] Aplet, L. J., and J. Wo Carson. "A Faraday effect optical isolator." Applied Optics 3.4 (1964): 544-545.
[6] Wang, Chen, Xiao-Lan Zhong, and Zhi-Yuan Li. "Linear and passive silicon optical isolator." Scientific reports 2.1 (2012): 1-6.
[7] Kawaguchi, Yuma, et al. "Optical isolator based on chiral light-matter interactions in a ring resonator integrating a dichroic magneto-optical material." Applied Physics Letters 118.24 (2021): 241104.
[8] Wu, X., et al. "Non-reciprocal bandpass filters using time-modulated resonators." IEEE Trans. Microw. Theory Tech (2018).
[9] Alvarez-Melcon, Alejandro, et al. "Coupling matrix representation of nonreciprocal filters based on time-modulated resonators." IEEE Transactions on Microwave Theory and Techniques 67.12 (2019): 4751-4763.
[10] Hadad, Yakir, Jason C. Soric, and Andrea Alu. "Breaking temporal symmetries for emission and absorption." Proceedings of the National Academy of Sciences 113.13 (2016): 3471-3475.
[11] Zang, Joachim Werner, et al. "Nonreciprocal wavefront engineering with time-modulated gradient metasurfaces." Physical Review Applied 11.5 (2019): 054054.
[12] Cheng, Lin, et al. "Superscattering, superabsorption, and nonreciprocity in nonlinear antennas." ACS Photonics 8.2 (2021): 585-591.
[13] Caloz, Christophe, et al. "Electromagnetic nonreciprocity." Physical Review Applied 10.4 (2018): 047001.
[14] Kahn, Frederic J., P. S. Pershan, and J. P. Remeika. "Ultraviolet magneto-optical properties of single-crystal orthoferrites, garnets, and other ferric oxide compounds." Physical review 186.3 (1969): 891.
[15] Adachi, Nobuyasu, et al. "Magneto-optical effect and ferromagnetic resonance of Bi–Fe garnet for high frequency electromagnetic sensor." Journal of Applied Physics 109.7 (2011): 07A506.
[16] Nazari, F., et al. "Optical isolation via $\mathcal{PT}$-symmetric nonlinear Fano resonances." Optics express 22.8 (2014): 9574-9584.
[17] Zhou, Xin, and Y. D. Chong. "PT symmetry breaking and nonlinear optical isolation in coupled microcavities." Optics express 24.7 (2016): 6916-6930.
[18] Correas-Serrano, Diego, N. K. Paul, and J. Sebastian Gomez-Diaz. "Plasmonic and photonic isolators based on the spatiotemporal modulation of graphene." Micro-and Nanotechnology Sensors, Systems, and Applications XI. Vol. 10982. International Society for Optics and Photonics, 2019.
[19] Correas-Serrano, D., Andrea Alù, and Juan Sebastian Gomez-Diaz. "Magnetic-free nonreciprocal photonic platform based on time-modulated graphene capacitors." Physical Review B 98.16 (2018): 165428.
[20] Yu, Zongfu, and Shanhui Fan. "Complete optical isolation created by indirect interband photonic transitions." Nature photonics 3.2 (2009): 91-94.
[21] Lira, Hugo, et al. "Electrically driven nonreciprocity induced by interband photonic transition on a silicon chip." Physical review letters 109.3 (2012): 033901.
[22] Sounas, Dimitrios L., Christophe Caloz, and Andrea Alu. "Giant non-reciprocity at the subwavelength scale using angular momentum-biased metamaterials." Nature communications 4.1 (2013): 1-7.
[23] Estep, Nicholas A., et al. "Magnetic-free non-reciprocity and isolation based on parametrically modulated coupled-resonator loops." Nature Physics 10.12 (2014): 923-927.
[24] Fleury, Romain, et al. "Sound isolation and giant linear nonreciprocity in a compact acoustic circulator." Science 343.6170 (2014): 516-519.
[25] Weis, Stefan, et al. "Optomechanically induced transparency." Science 330.6010 (2010): 1520-1523.
[26] Morgado, Tiago A., and Mário G. Silveirinha. "Nonlocal effects and enhanced nonreciprocity in current-driven graphene systems." *Physical Review B* 102.7 (2020): 075102.
[27] Shastri, Kunal, Mohamed Ismail Abdelrahman, and Francesco Monticone. "Nonreciprocal and topological plasmonics." *Photonics*. Vol. 8. No. 4. MDPI, 2021.
[28] Maier, Stefan A., ed. *World Scientific Handbook Of Metamaterials And Plasmonics (In 4 Volumes)*. Vol. 16. World scientific, 2017.

[29] Stewart, Matthew E., et al. "Nanostructured plasmonic sensors." *Chemical reviews* 108.2 (2008): 494-521.
[30] Le Ru, Eric, and Pablo Etchegoin. *Principles of Surface-Enhanced Raman Spectroscopy: and related plasmonic effects*. Elsevier, 2008.
[31] Tokel, Onur, Fatih Inci, and Utkan Demirci. "Advances in plasmonic technologies for point of care applications." *Chemical reviews* 114.11 (2014): 5728-5752.
[32] Novotny, Lukas, and Bert Hecht. *Principles of nano-optics*. Cambridge university press, 2012.
[33] Grigorenko, Alexander N., Marco Polini, and K. S. Novoselov. "Graphene plasmonics." *Nature photonics* 6.11 (2012): 749-758.
[34] Tamagnone, Michele, et al. "Reconfigurable terahertz plasmonic antenna concept using a graphene stack." *Applied Physics Letters* 101.21 (2012).
[35] Gómez-Díaz, Juan-Sebastian, and Julien Perruisseau-Carrier. "Graphene-based plasmonic switches at near infrared frequencies." *Optics express* 21.13 (2013): 15490-15504.
[36] Nemilentsau, Andrei, Tony Low, and George Hanson. "Anisotropic 2D materials for tunable hyperbolic plasmonics." *Physical review letters* 116.6 (2016): 066804.
[37] Chen, Wei Ting, Alexander Y. Zhu, and Federico Capasso. "Flat optics with dispersion-engineered metasurfaces." *Nature Reviews Materials* 5.8 (2020): 604-620.
[38] Manzeli, Sajedeh, et al. "2D transition metal dichalcogenides." *Nature Reviews Materials* 2.8 (2017): 1-15.
[39] Li, Guixin, Shuang Zhang, and Thomas Zentgraf. "Nonlinear photonic metasurfaces." *Nature Reviews Materials* 2.5 (2017): 1-14.
[40] Meinzer, Nina, William L. Barnes, and Ian R. Hooper. "Plasmonic meta-atoms and metasurfaces." *Nature photonics* 8.12 (2014): 889-898.
[41] Xia, Fengnian, et al. "Two-dimensional material nanophotonics." *Nature Photonics* 8.12 (2014): 899-907.
[42] Hassani Gangaraj, S. Ali, et al. "Enhanced Nonlinear Optical Effects in Drift-Biased Nonreciprocal Graphene Plasmonics." *ACS Photonics* (2023).
[43] Schaug-Pettersen, T., and A. Tonning. "On the optimum performance of variable and nonreciprocal networks." *IRE Transactions on Circuit Theory* 6.2 (1959): 150-158.
[44] Zanotto, Simone, Francesco Morichetti, and Andrea Melloni. "Fundamental limits on the losses of phase and amplitude optical actuators." *Laser & Photonics Reviews* 9.6 (2015): 666-673.
[45] Tamagnone, Michele, et al. "Fundamental limits and near-optimal design of graphene modulators and non-reciprocal devices." *Nature photonics* 8.7 (2014): 556-563.
[46] Vakil, Ashkan, and Nader Engheta. "Transformation optics using graphene." *Science* 332.6035 (2011): 1291-1294.
[47] Zhao, Dan, et al. "Tunable On-Chip Terahertz Isolator Based on Nonreciprocal Transverse Edge Spin State of Asymmetric Magneto-Plasmonic Waveguide." *Laser & Photonics Reviews* 17.2 (2023): 2200509.
[48] Hanson, George W. "Dyadic Green's functions for an anisotropic, non-local model of biased graphene." *IEEE Transactions on antennas and propagation* 56.3 (2008): 747-757.
[49] Lovat, Giampiero, et al. "Non-local models and effects in graphene nanointerconnects." *2013 International Symposium on Electromagnetic Compatibility*. IEEE, 2013.
[50] Correas-Serrano, D., et al. "Black phosphorus plasmonics: anisotropic elliptical propagation and nonlocality-induced canalization." *Journal of Optics* 18.10 (2016): 104006.
[51] Zhao, Wenyu, et al. "Efficient Fizeau drag from Dirac electrons in monolayer graphene." *Nature* 594.7864 (2021): 517-521.
[52] Morgado, Tiago A., and Mário G. Silveirinha. "Directional dependence of the plasmonic gain and nonreciprocity in drift-current biased graphene." *Nanophotonics* 11.21 (2022): 4929-4936.
[53] Correas-Serrano, D., and J. S. Gomez-Diaz. "Nonreciprocal and collimated surface plasmons in drift-biased graphene metasurfaces." *Physical Review B* 100.8 (2019): 081410.
[54] Chang, You-Chia, et al. "Realization of mid-infrared graphene hyperbolic metamaterials." *Nature communications* 7.1 (2016): 10568.
[55] Morgado, Tiago A., and Mário G. Silveirinha. "Drift-induced unidirectional graphene plasmons." *ACS photonics* 5.11 (2018): 4253-4258.
[56] Morgado, Tiago A., and Mário G. Silveirinha. "Drift-induced Nonreciprocal Graphene Plasmonics." *2019 PhotonIcs & Electromagnetics Research Symposium-Spring (PIERS-Spring)*. IEEE, 2019.
[57] Hassani Gangaraj, S. Ali, and Francesco Monticone. "Drifting electrons: Nonreciprocal plasmonics and thermal photonics." *ACS photonics* 9.3 (2022): 806-819.
[58] Paul, N. K., and J. S. Gomez-Diaz. "Broadband and unidirectional plasmonic hyperlensing in drift-biased graphene." *Applied Physics Letters* 118.9 (2021).
[59] Morgado, Tiago A., and Mário G. Silveirinha. "Negative Landau damping in bilayer graphene." *Physical review letters* 119.13 (2017): 133901.
[60] Dong, Yinan, et al. "Fizeau drag in graphene plasmonics." *Nature* 594.7864 (2021): 513-516.
[61] Navajas, David, et al. "Addressing the Impact of Surface Roughness on Epsilon-Near-Zero Silicon Carbide Substrates." *ACS photonics* 10.9 (2023): 3105-3114.
[62] Pérez-Escudero, José M., et al. "Silicon carbide as a material-based high-impedance surface for enhanced absorption within ultra-thin metallic films." *Optics Express* 28.21 (2020): 31624-31636.
[63] Hanson, George W. "Dyadic Green's functions and guided surface waves for a surface conductivity model of graphene." *Journal of Applied Physics* 103.6 (2008).
[64] Correas-Serrano, Diego, et al. "Spatially dispersive graphene single and parallel plate waveguides: Analysis and circuit model." *IEEE Transactions on Microwave Theory and Techniques* 61.12 (2013): 4333-4344.
[65] Lovat, Giampiero, et al. "Semiclassical spatially dispersive intraband conductivity tensor and quantum capacitance of graphene." *Physical Review B* 87.11 (2013): 115429.
[66] Correas-Serrano, D., et al. "Nonlocal response of hyperbolic metasurfaces." *Optics Express* 23.23 (2015): 29434-29448.
[67] Correas-Serrano, Diego, et al. "Graphene-based plasmonic tunable low-pass filters in the terahertz band." *IEEE Transactions on Nanotechnology* 13.6 (2014): 1145-1153.
[68] "COMSOL Multiphysics Reference Manual, version 6.0", COMSOL, Inc, www.comsol.com .
[69] Pozar, David M. *Microwave engineering*. John wiley & sons, 2011.
[70] Gerber, Justin A., et al. "Phase-resolved surface plasmon interferometry of graphene." *Physical review letters* 113.5 (2014): 055502.
[71] Alonso-González, Pablo, et al. "Acoustic terahertz graphene plasmons revealed by photocurrent nanoscopy." *Nature nanotechnology* 12.1 (2017): 31-35.
[72] Chen, Jianing, et al. "Optical nano-imaging of gate-tunable graphene plasmons." *Nature* 487.7405 (2012): 77-81.
[73] Gomez-Diaz, J. S., and Andrea Alu. "Flatland optics with hyperbolic metasurfaces." *ACS Photonics* 3.12 (2016): 2211-2224.
[74] Crassee, Iris, et al. "Giant Faraday rotation in single-and multilayer graphene." *Nature Physics* 7.1 (2011): 48-51.
[75] Poumirol, Jean-Marie, et al. "Electrically controlled terahertz magneto-optical phenomena in continuous and patterned graphene." *Nature communications* 8.1 (2017): 14626.
[76] Tamagnone, Michele, et al. "Magnetoplasmonic enhancement of Faraday rotation in patterned graphene metasurfaces." *Physical Review B* 97.24 (2018): 241410.
[77] Tamagnone, Michele, et al. "Near optimal graphene terahertz non-reciprocal isolator." *Nature communications* 7.1 (2016): 11216.
[78] Sounas, Dimitrios L., and Christophe Caloz. "Edge surface modes in magnetically biased chemically doped graphene strips." *Applied Physics Letters* 99.23 (2011): 231902.
[79] Dmitriev, Victor, and Samara L. Matos da Silva. "Ultra wideband THz graphene four-port circulators." *Microwave and Optical Technology Letters* 62.1 (2020): 112-117.
[80] Schaibley, John R., et al. "Valleytronics in 2D materials." *Nature Reviews Materials* 1.11 (2016): 1-15.
[81] Cao, Ting, et al. "Valley-selective circular dichroism of monolayer molybdenum disulphide." *Nature communications* 3.1 (2012): 887.
[82] Yin, Jianbo, et al. "Tunable and giant valley-selective Hall effect in gapped bilayer graphene." *Science* 375.6587 (2022): 1398-1402.
[83] Zayets, Vadym, et al. "Optical isolator utilizing surface plasmons." *Materials* 5.5 (2012): 857-871.
[84] Klein, Matthew, et al. "2D semiconductor nonlinear plasmonic modulators." *Nature communications* 10.1 (2019): 3264.